Radar Ranging of the Planet Mars at 8495 MHz

G. S. Downs and P. E. Reichley
Communications Systems Research Section

A simulation was performed for the radar system in order to ensure detection of the planet Mars at the start of the 1975 series of radar probes of the surface. Appropriate parameters were found. Appropriate parameters were also found for use at opposition (December 1975). Systematic errors in the measured delay with changes in surface roughness were observed. This effect is shown to be many times larger than the expected rms fluctuations in the measured delays.

I. Introduction

The surface of the planet Mars will be probed with S- and X-band radar signals during 1975 and 1976, all in preparation for the landing of two spacecraft in 1976. The measurements to be performed at JPL will use the R & D radar system at DSS 14, Goldstone, California, at a frequency of 8495 MHz. In preparation, several series of radar data sets were simulated and processed. That is, the expected power in the reflected signal was calculated as a function of time delay and frequency for several sets of radar system parameters. The random fluctuations caused by receiver noise were superimposed using a random number generator. The appropriate signal-to-noise ratio was calculated for certain distances to the planet, assuming appropriate X-band antenna parameters. The round-trip time delay of the signal reflected from the surface of the planet was determined. Up to 120 delay measurements were made to allow determination of the detection probability and the measurement accuracy. An appropriate set of radar parameters was chosen in light of the results of this study.

II. How Delay Is Measured

The basic radar data set consists of a matrix of received power as a function of time delay and excess doppler shift. Separate regions on the surface will exhibit separate time delays because of the spherical shape of the planet.

Let θ represent the angle between the line of sight from the radar to the center of the planet and the radius to the point on the surface. The time delay τ of the signal reflected from that surface point back to the radar is given by

$$\tau = \frac{2R}{c}(1 - \cos\theta) + \frac{2D}{c} \tag{1}$$

where R is the radius of the planet and c is the speed of light; D is the distance along the line of sight to the closest point on the surface. Note that θ is also the angle of incidence of the signal on the surface. θ and D are each functions of time. The large delay due to D is removed at the time of data collection. The small changes in θ due to the relative motion of Mars and Earth in the time interval $2D/c$ are neglected. The locus of a curve of a constant τ is a circle in the plane perpendicular to the line of sight and whose center lies on the line of sight. Regions of a particular delay are isolated by modulating the phase of the transmitted signal with a pseudorandom binary code. If the bit length of the code is T seconds, the normalized cross correlation function of the transmitted signal with the received signal is given by

$$R_r(\tau) \approx \begin{cases} 1 - \dfrac{1}{T}|\tau - \tau_0|; & |\tau - \tau_0| \leq T \\ 0 \qquad\qquad\quad ; & |\tau - \tau_0| > T \end{cases} \tag{2}$$

where τ_0 is the round trip delay. A band of surface elements located within T seconds of τ_0 can be isolated. In practice, the received signal is passed through a bank of correlators, the ith corresponding to a round trip delay τ_{0i}. The power in the output of the ith correlator is then the sum of the power in the reflected signals corresponding to the delays $\tau_{0i} - T \leq \tau \leq \tau_{0i} + T$, each delay component being weighted by the range window $R(\tau) = R_r^2(\tau)$. There is an ambiguity in the delay τ_0 of the reflected signal which is equal to the length of the binary code. That is, $R(\tau)$ is periodic in time mT, where m is the number of bits in the code. Usually the planetary ephemeris is good enough to resolve this ambiguity in time delay. There remains, however, a small perturbation to the total reflected power from the region defined by $R(\tau_{0i})$ since contributions are obtained from all regions centered at $\tau = \tau_{0i} \pm nmT$, where n is any integer.

Further resolution of the planet's surface is usually obtained by taking advantage of the doppler spreading of the reflected signal caused by the rotation of Mars. Loci of constant doppler shift are circles on the surface, parallel to the plane defined by the apparent spin axis of the planet and the line of sight. The intersections of the circles of constant range and the circles of constant doppler shift then isolate particular small regions on the surface (see Fig. 1). Therefore, the discrete power spectrum of the output of each correlator is estimated using discrete time samples. The power at each discrete frequency f_0 in the spectrum is in fact the sum of power from regions of varying doppler shift f. Each region is weighted by the familiar function

$$D(f) = \frac{\sin^2[\pi N(f - f_0)/\Delta f]}{N^2 \sin^2[\pi(f - f_0)/\Delta f]} \tag{3}$$

where $\overline{N}$ is the number of discrete frequencies, separated by Δf, in the power spectrum.

The delay-doppler geometry imposed on the planet's surface is pictured in Fig. 1, where the planet is viewed from the direction of the apparent spin axis. The angle of incidence θ is the angle between the direction to Earth and N, the local normal to the mean sphere. The shape of the range window $R(\tau)$ is shown at the left for the case of $T = 6$ μs. The shape of the doppler window $D(f)$ is shown at the right for the case of $\Delta f = 10.2$ Hz, when $\lambda = 12.55$ cm. As is often the case in these measurements, the correlators are separated such that $\tau_{0(i+1)} - \tau_{0i} = T/2$. Note that as the planet rotates, any given region near the doppler equator (a great circle perpendicular to the circles of constant doppler shift and bisecting the rings of constant range) is probed at a variety of angles of incidence. Each set of received power as a function of delay and doppler (a data frame) represents a snapshot of the surface near the doppler equator. An example of such a data frame appears in Fig. 2.

Consider for the moment the power vs time delay at a fixed doppler shift. The reflected power corresponds to a narrow region at a particular longitude and a minimum angle of incidence. The location of the planet at that particular doppler shift is taken to be the delay at which the power is a maximum. As the planet rotates, a series of delay functions corresponding to particular values of θ become available for a particular longitude. With the extra delay due to curvature of the surface removed, the collection of delay functions is usually added to produce a composite delay function in which the signal-to-noise ratio is larger. The delay corresponding to the peak power then defines the distance to the planet.

In practice, the presence of noise will cause errors in locating the planet. Also, the weak signal case gives rise to a finite possibility of a false detection of the planet.

The following discussion is devoted to a determination of the probability of a correct detection and the measurement error, once detection has been established. These probabilities and errors are dependent on the signal-to-noise ratio, which in turn is dependent on the parameters of the radar system and the surface characteristics. The radar system parameters and surface characteristics are varied over an appropriate range in the discussion below.

III. The Data

An example of simulated data is presented in Fig. 2. The spectrum of the output of 32 correlators is presented in Fig. 2(a) for the noise-free case. The magnitudes of the spectral components are proportional to the received power expected for the case of $T = 6\ \mu s$ and $\Delta f = 36.2$ Hz at $\lambda = 3.53$ cm. Note that correlators are offset progressively in delay by $T/2 = 3\ \mu s$. These magnitudes were calculated by evaluating the radar equation:

$$P(f_0,\tau_0) = \frac{P_x G_x G_r \lambda^2}{64\,\pi^3 D^4} \cdot \frac{\rho_0 C}{2} \iint_{S(f,\tau)} ds \frac{R(\tau - \tau_0)\, D(f - f_0)}{[\cos^4 \theta + C \sin^2 \theta]^{3/2}} \tag{4}$$

where P_x and G_x are the transmitting power and antenna gain, respectively. G_r is the receiving antenna gain. The transmitter operates at wavelength λ. The planet, located at distance D, is characterized by a reflectivity ρ_0 and roughness parameter C. The denominator of the integrand in Eq. (4) (sometimes called the Hagfors backscatter function, Refs. 1 and 2) describes how the power scattered back toward the receiver varies with the angle of incidence, where θ is now a function τ and f. The surface S over which the integration takes place is determined by the position of the range and doppler windows relative to the planet. The details of the evaluation of the integral, and in particular the effects of aliasing in frequency and ambiguity in range will be discussed in a forthcoming article.

The received power $P(f,\tau)$ was calculated for 32 delays and 64 frequencies for values of $\Delta f = 36.2$, 72.5 and 145 Hz with $T = 6\ \mu s$ and for $\Delta f = 145$ Hz with $T = 12\ \mu s$. In each case, $\tau_{0(i+1)} - \tau_{0i} = \Delta\tau = T/2$. In the case of Mars, these values of Δf correspond to $N - S$ slices on the surface of widths of 0.16, 0.32 and 0.64 deg in longitude, respectively. The transmitter power P_x was taken to be 400 kW, operating at 8495 MHz, so $\lambda = 3.53$ cm. The gains G_x and G_r were taken to be equal, and these values were deduced from data provided by Freiley (Ref. 3). A nominal value of system efficiency of 0.40 was assumed from the data of Ref. 3. This value corresponds to a value 1 σ lower than the mean transmit system efficiency at an elevation of 70 deg. The corresponding antenna gains are 71.1 dB. The 4 sets of values of $(\Delta f,\tau)$ were subdivided into sets of different values of D, where D varied between 0.56 AU (closest approach during the 1975 opposition) and 1.5 AU. These subsets were, in turn, subdivided even further to correspond to roughness $C = 50$, 150, 300, 1000, 2000 and 5000. A total of 78 distinct sets of data frames were then generated from Eq. (4). A value of $\rho_0 = 0.08$ was assumed for all evaluations of Eq. (4). This value is an average obtained from previous radar probes of Mars. Although ρ_0 varies between 0.01 and 0.15, most regions have a reflectivity close to 0.08.

In practice, data frames similar to those of Fig. 2(b) are measured at regular time intervals. To improve the signal-to-noise ratio, several sequential data frames are usually added together. The magnitude of each spectral component then represents an energy. That is, a signal of intensity $P = P(f,\tau)$ watts is integrated for t_I seconds to produce Pt_I joules. Now, t_I should be long enough to allow a particular region on the planet's surface to rotate from one discrete doppler frequency to the next. In this analysis, t_I was chosen such that the planet rotated about 0.75 of that distance. For example, when $\Delta f = 36.2$ Hz (0.16 deg in longitude), t_I was chosen to be 30 seconds, an interval in which the planet rotates 0.12 deg.

The superimposing of a noisy signal of the proper magnitude was performed in the following manner. A series of random numbers with a variance of 1.0 was generated. The scale of the variance was chosen by noting that the receiver noise power is $kT_s\Delta f$ watts for each spectral component, where k is Botzmann's constant and T_s is the system noise temperature. In time t_I the mean energy obtained by integrating this component of the noise is $kT_s\Delta ft_I$ and the variance associated with the measurement of this component is $(kT_s)^2\Delta ft_I$. The measurement of the planetary component Pt_I also is subject to random fluctuations. The total variance is calculated assuming that the wideband receiver component and the planetary component are each nearly Gaussian random processes. (They are in fact Rayleigh processes in which the mean is much larger than the root-mean-square fluctuation.) The total variance is then $(kT_s)^2\Delta ft_I + (Pt_I)^2/\Delta ft_I$.

In the generation of the series of random numbers it was assumed that $Pt_I << kT\Delta ft_I$, so that the planetary component of the variance could be ignored. The series of random numbers, so scaled, and the mean value of the receiver noise were added to the function $P(f,\tau)$ to obtain a simulated data frame. T_s was taken to be 23 K. A data frame similar to Fig. 2(b) was generated from the noise-free frame of Fig. 2(a) in the above manner. The data in Fig. 2(b) correspond to $D = 0.56$ AU and $C = 300$. The constant wide-band component of the receiver noise has been subtracted. A total of 70 data frames containing independent additive noise, representing integrations over t_I seconds, were generated to provide a good measure of the statistics of interest.

IV. The Delay Measurements

In practice, one cannot probe the planet's surface with a monostatic radar system (one antenna) on a continuous basis, since the transmitter must be turned off during reception. Hence, the simulated data frames were arranged in time to duplicate the case in which the radar signal is transmitted for a time interval equal to the round-trip time between Earth and Mars, and then received for one round-trip time. Reception immediately follows transmission for an equal time interval. Clearly, in one round-trip time one will usually collect several data frames, each representing an integration of t_I seconds. Since the transmitter is not on continuously, only ½ of the available angles of incidence will be probed. A view window, of width equal to the amount of rotation accomplished in one round-trip time, slides over the surface allowing some angles of incidence and omitting others.

The results of the delay measurements are presented in Tables 1-4. At first, the radar system parameters T and Δf were chosen to be equal to those used in earlier work on Mars at 2388 MHz. The doppler shifts were scaled from 2388 to 8495 MHz such that Δf corresponded to a longitude interval ΔL of 0.16 deg. At each of the four values of D in Table 1, six values of roughness C were chosen to cover the range expected at 8495 MHz. A number N_T (between 90 and 120) composite delay functions, each representing a different mixture of angles of incidence, were available for each combination of D and C. If the peak amplitude of a composite delay function was 2.5 to 3 times larger than the rms noise level, the planet was considered detected and the corresponding delay τ was recorded. However, in N_D detections, a certain number N_F are false detections which usually occur in the weak signal case. Values of τ which placed the planet more than T μs away from the known position of the planet were considered false detections. The fraction P_d of successful detections and the fraction P_e of these detections that were false are listed in Table 1 and calculated from

$$\begin{aligned} P_d &= \frac{N_D - N_F}{N_T} \\ P_e &= \frac{N_F}{N_D} \end{aligned} \qquad (5)$$

The values of N_D, the mean τ_{b0} in the range estimates, and the associated rms fluctuation σ_{T0} presented in Table 1 represent averages over all the available data. However, some of the composite delay functions contain contributions from angles of incidence primarily near 0 deg (the maximum is about 2 deg in this simulation). These delay functions were isolated and, finding N_c of them, the mean τ_{bc} of this set and the associated rms fluctuations σ_{Tc} were calculated and listed in Table 1.

The true mean and variance are represented by τ_{bc} and σ_{Tc}. The reason for this can be understood by examining Fig. 3. The delay τ of each composite delay function has been presented vs the centroid $\bar{n}_d$ of the angle-of-incidence view window. The centroid is expressed in units of ΔL (or Δf). In Fig. 3, where $C = 5000$, the shape of the backscatter function changes rapidly with θ, so the shape of the delay function flattens markedly as $\bar{n}_d$ increases. A positive drift in the delay of the peak amplitude and a decrease in the magnitude of the peak accompany this flattening. The positive drift is readily observable in Fig. 3(a). Noise fluctuations are low since the corresponding distance is only 0.56 AU. The distance is 1.14 AU in Fig. 3(b), and the larger scatter in τ for $\bar{n}_d > 6$ is evidence of the decreasing peak amplitude. By includinly only the values of τ for which $\bar{n}_d < 6$ in the statistics, a true representation of the measurement accuracy is obtained. Including all available values of τ produces a larger variance because of the systematic drift in τ with window position.

The mean τ_{bc} is a function of the roughness parameter C. In Fig. 4(a) the measurements of τ are presented vs $\bar{n}_d$ for $C = 150$ at a distance of 0.56 AU. The drift in τ with $\bar{n}_d$ is not as extreme as in Fig. 3(a) since the backscatter function varies more slowly with θ. Note however that τ_{bc} for $\bar{n}_d < 6$ is not identical to the similar value in Fig. 3(a). This bias is again caused by the retarded, flatter delay functions characteristic of low values of C or larger values of θ. The data of Fig. 4(b), corresponding to $D = 0.8$ AU, show how small signal-to-noise ratios mask the effects discussed above.

At opposition $D = 0.56$ AU. The results of Table 1 indicate that maximum ranging accuracies of 40 to 300 ns can be obtained. The systematic changes of τ with $\overline{n}_d$ and C are large compared to these hypothetical accuracies. It will then be desirable to apply corrections to the estimates of τ to obtain the minimum possible rms fluctuations.

The data of Tables 3–4 were obtained in a search of the data-frame parameters which ensure detection of the planet Mars at the start of the 1975 series of measurements (during August, when Mars is at 1.2 AU). The parameters underlying Table 4 ($T = 12$ μs, $\Delta L = 0.64$ deg) provide a reasonable probability of detection of rough as well as smooth surfaces at 1.2 AU. These are the parameters to be used at the start of the series of measurements. Tables 2 and 3 are useful as an aid in determining what T and ΔL should be as Mars progresses towards opposition.

References

1. Hagfors, T., "Backscattering from an Undulating Surface with Applications to Radar Returns from the Moon," *JGR*, 69, pp. 3779–3784, 1964.
2. Hagfors, T., *Radar Astronomy*, Evans, J. V., and Hagfors, T., eds., Chapter 4, pp. 187–218, McGraw-Hill, New York, 1968.
3. Freiley, A. J., "DSS-14 XKR Cone Performance," JPL Interoffice Memo No. 3331-75-001, Mar. 10, 1975 (an internal document).

Table 1. Detection probability and σ_T for $T = 6$ μs, $\Delta L = 0.16$ deg, $\rho_0 = 0.08$

D, AU	C	P_d, %	P_e, %	N_D	σ_{T0}, μs	τ_{b0}, μs	N_c	σ_{Tc}, μs	τ_{bc}, μs
0.56	50	98	1	118	0.44	2.6	64	0.30	2.4
	150	100	0	120	0.26	2.4	64	0.12	2.25
	300	100	0	120	0.31	2.3	64	0.08	2.1
	1000	100	0	120	0.31	2.0	64	0.09	1.75
	2000	100	0	120	0.38	1.7	56	0.04	1.4
	5000	100	0	120	0.45	1.4	56	0.04	1.1
0.80	50	56	10	65	1.33	–	40	1.38	–
	150	97	0	113	0.65	–	61	0.42	–
	300	100	0	117	0.62	–	61	0.15	–
	1000	100	0	117	0.39	–	61	0.11	–
	2000	100	0	117	0.40	–	55	0.04	–
	5000	100	0	117	0.54	–	55	0.04	–
1.00	50	3	57	4	1.80	–	–	–	–
	150	62	1	76	1.18	–	42	0.98	–
	300	83	1	102	0.72	–	54	0.57	
	1000	95	0	117	0.62	–	58	0.33	–
	2000	95	0	117	0.55	–	55	0.32	–
	5000	92	0	113	0.57	–	52	0.22	–
1.14	50	2	50	2	1.34	–	–	–	–
	150	38	10	38	1.52	–	29	1.44	–
	300	73	3	73	0.94	–	39	0.80	–
	1000	86	0	86	0.45	–	50	0.38	–
	2000	91	0	91	0.54	–	52	0.45	–
	5000	88	0	88	0.50	–	49	0.35	–

Table 2. Detection probability and σ_T for $T = 6$ μs, $\Delta L = 0.32$ deg, $\rho_0 = 0.08$

D, AU	C	P_d, %	P_e, %	N_D	σ_{T0}, μs	τ_{b0}, μs	N_c	σ_{Tc}, μs	τ_{bc}, μs
1.00	50	12	–	13	1.47	–	8	1.18	–
	150	81	3	91	1.09	2.5	56	1.24	2.5
	300	82	3	83	0.81	2.5	46	0.68	2.5
	1000	93	0	94	0.61	2.0	52	0.58	2.0
	2000	94	0	95	0.49	1.6	47	0.56	1.6
	5000	93	0	94	0.74	1.5	46	0.54	1.2
1.14	50	4	–	4	1.15	–	–	–	–
	150	60	6	61	1.50	–	34	1.50	–
	300	82	3	83	0.81	–	46	0.68	–
	1000	93	0	94	0.61	–	52	0.58	–
	2000	94	0	95	0.49	–	47	0.56	–
	5000	93	0	94	0.74	–	46	0.54	–
1.50	50	–	–	–	–	–	–	–	–
	150	–	–	–	–	–	–	–	–
	300	30	10	26	1.37	–	20	1.28	–
	1000	76	0	67	0.53	–	41	0.59	–
	2000	83	0	73	0.63	–	37	0.65	–
	5000	84	0	74	0.45	–	37	0.51	–

Table 3. Detection probability and σ_T for $T = 6$ μs, $\Delta L = 0.64$ deg, $\rho_0 = 0.08$

D, AU	C	P_d, %	P_e, %	N_D	σ_{T0}, μs	τ_{b0}, μs	N_c	σ_{Tc}, μs	τ_{bc}, μs
1.00	50	46	12	49	1.92	3.3	31	1.72	3.1
	150	92	1	98	0.93	2.7	65	0.98	2.9
	300	100	0	106	1.00	2.7	70	0.65	2.6
	1000	100	0	106	0.91	2.2	70	0.51	2.0
	2000	100	0	106	0.61	1.7	53	0.29	1.5
	5000	100	0	106	0.67	1.4	53	0.20	1.1
1.14	50	11	31	10	1.60	–	6	2.0	–
	150	78	6	74	1.50	–	48	1.55	–
	300	95	0	90	1.00	–	57	0.84	–
	1000	100	0	95	0.75	–	62	0.53	–
	2000	100	0	94	0.64	–	49	0.56	–
	5000	98	1	93	0.71	–	50	0.82	–
1.50	50	–	–	–	–	–	–	–	–
	150	9	–	8	1.5	–	7	1.40	–
	300	49	5	44	1.62	–	27	1.20	–
	1000	78	0	69	0.72	–	44	0.65	–
	2000	80	0	71	0.47	–	37	0.46	–
	5000	84	0	75	0.64	–	37	0.25	–

Table 4. Detection probability and σ_τ for $T = 12$ μs, $\Delta L = 0.64$ deg, $\rho_0 = 0.08$

D, AU	C	P_d, %	P_e, %	N_D	$\sigma_{\tau 0}$, μs	τ_{b0}, μs	N_c	$\sigma_{\tau c}$, μs	τ_{bc}, μs
1.00	50	82	4	91	2.62	5.4	86	2.66	5.4
	150	100	0	111	1.48	5.0	103	1.50	5.0
	300	100	0	111	1.10	4.4	103	0.74	4.4
	1000	100	0	111	0.78	3.4	103	0.70	3.2
	2000	100	0	111	1.12	2.8	53	0.32	2.4
	5000	100	0	111	1.48	7.0	53	0.36	1.6
1.14	50	44	10	49	3.40	–	30	3.40	–
	150	91	2	101	2.00	–	63	2.20	–
	300	98	1	109	1.75	–	70	1.96	–
	1000	100	0	111	1.28	–	71	0.92	–
	2000	98	0	109	1.44	–	55	0.77	–
	5000	95	0	106	0.93	–	51	1.14	–
1.50	50	–	–	–	–	–	–	–	–
	150	30	10	30	3.10	–	19	3.60	–
	300	68	0	69	1.84	–	42	1.92	–
	1000	76	1	77	1.08	–	44	1.10	–
	2000	80	0	81	1.08	–	38	1.38	–
	5000	80	0	80	1.04	–	37	1.30	–

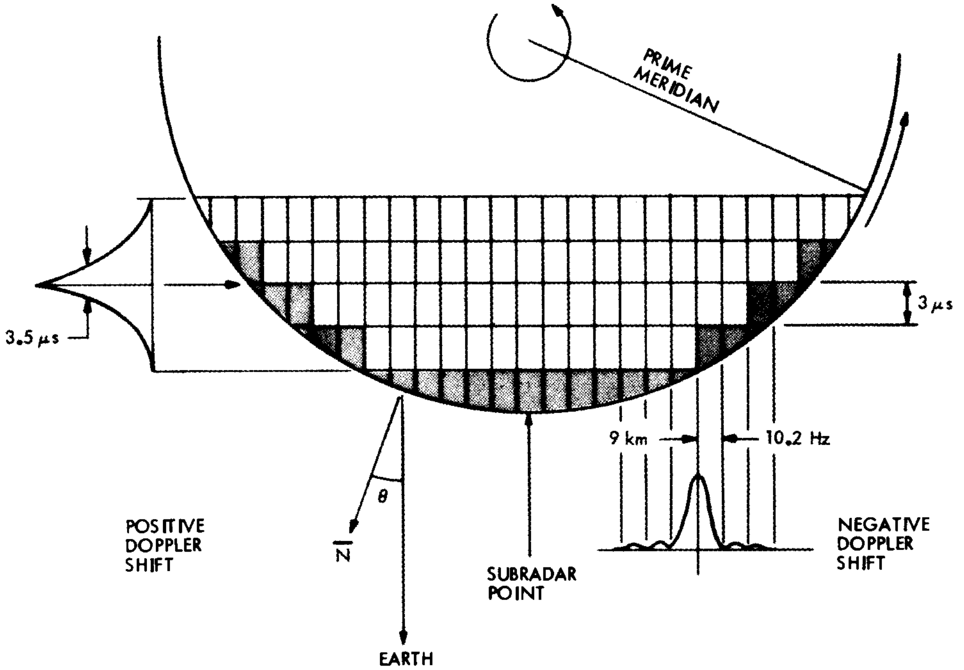

Fig. 1. Partitioning of Mars by the radar system

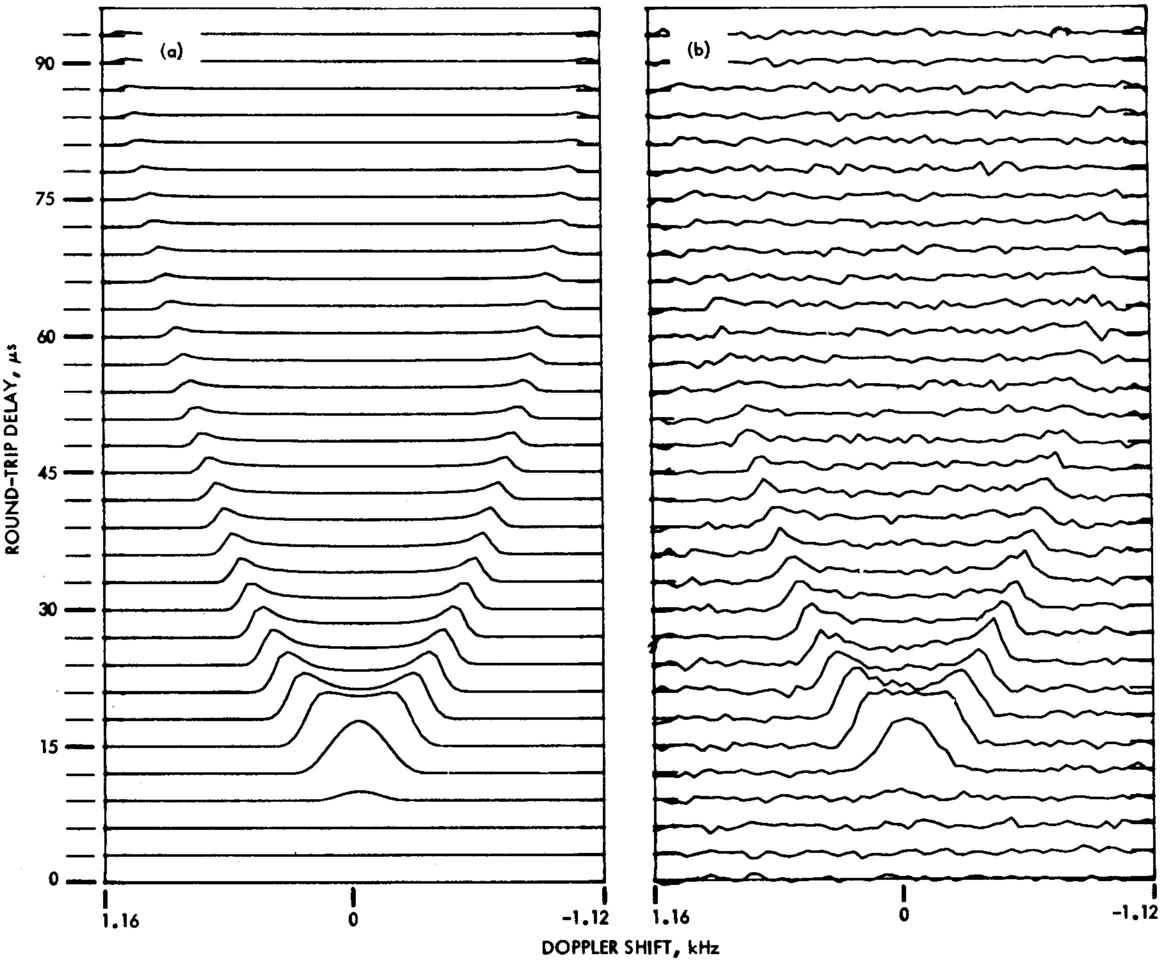

Fig. 2. Received power vs doppler shift and delay for $\Delta f = 36.2$ Hz, $T = 6 \mu s$, $\rho_0 = 0.08$, and $C = 300$: (a) noise-free case, (b) noisy case (see text for noise parameters)

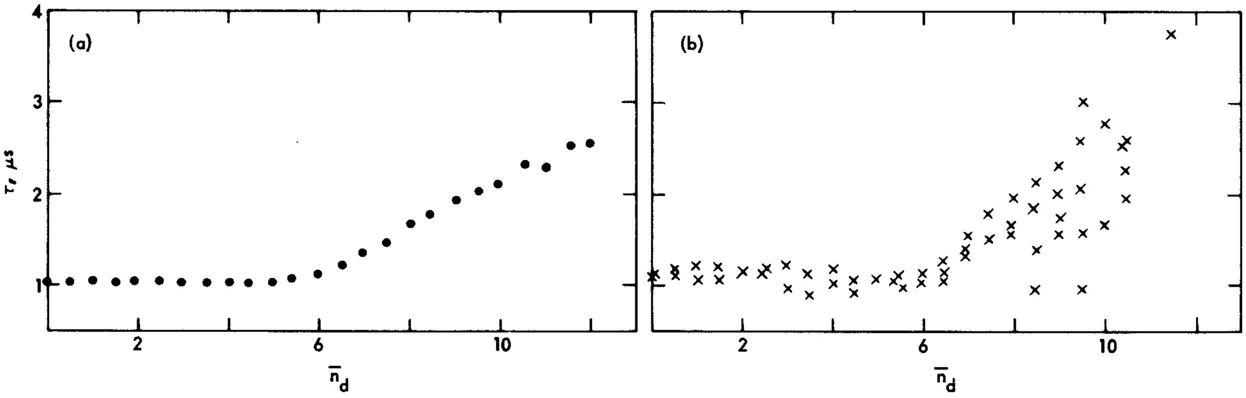

Fig. 3. Estimation of τ vs the centroid $\bar{n}_d$ of the angle-of-incidence window for $C = 5000$: (a) $D = 0.56$ AU, (b) $D = 1.14$ AU

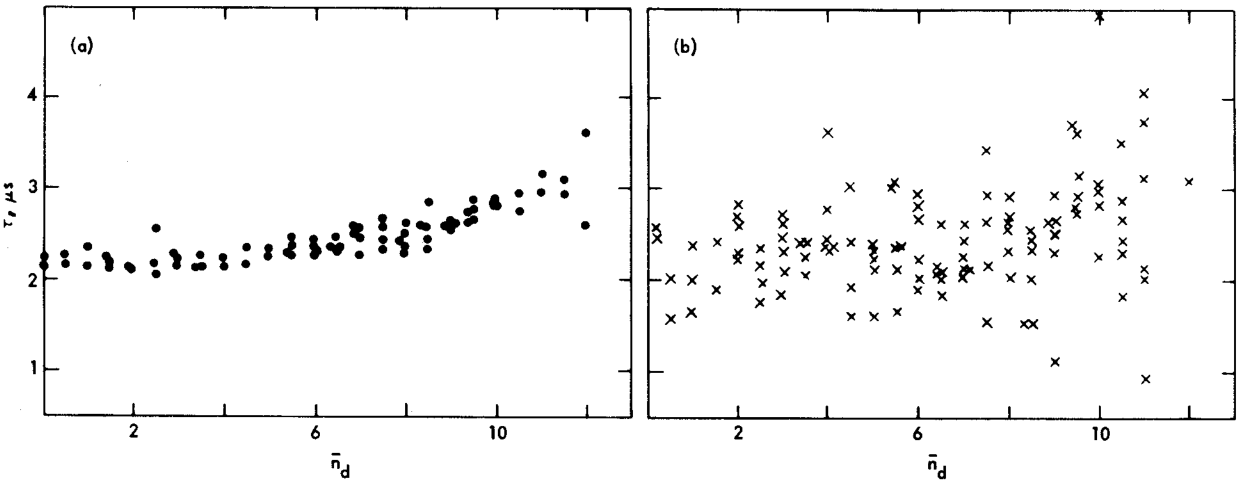

Fig. 4. Estimation of τ vs the centroid $\bar{n}_d$ of the angle-of-incidence window for $C = 150$: (a) $D = 0.56$ AU, (b) $D = 0.8$ AU